Remote Sensing of Environment 115 (2011) 2976–2985

Contents lists available at ScienceDirect

Remote Sensing of Environment

journal homepage: www.elsevier.com/locate/rse

Segmentation optimization and stratified object-based analysis for semi-automated geomorphological mapping

Niels S. Anders *, Arie C. Seijmonsbergen, Willem Bouten

Institute for Biodiversity and Ecosystem Dynamics, Computational Geo-Ecology, University of Amsterdam, PO Box 94248, 1090 GE, The Netherlands

ARTICLE INFO

Article history:
Received 19 January 2011
Received in revised form 13 May 2011
Accepted 14 May 2011
Available online 11 June 2011

Keywords:
Geomorphometry
OBIA
LiDAR
Vorarlberg
Austria

ABSTRACT

Semi-automated geomorphological mapping techniques are gradually replacing classical techniques due to increasing availability of high-quality digital topographic data. In order to efficiently analyze such large amounts of data, there is a need for optimizing the processing of automated mapping techniques. In this context, we present a novel approach to semi-automatically map alpine geomorphology using stratified object-based image analysis. We used a 1 m Digital Terrain Model (DTM) derived from laser altimetry data from a mountainous catchment from which we calculated various Land-Surface Parameters (LSPs). The LSPs 'slope angle' and 'topographic openness' have been combined into a single composite layer for selecting reference material and delineating training samples. We developed a novel method to semi-automatically assess segmentation results by comparing 2D frequency distribution matrices of training samples and image objects. The segmentation accuracy assessment allowed us to automate optimization of the scale parameter and LSPs used for segmentation. We concluded that different geomorphological feature types have different sets of optimal segmentation parameters. The feature-dependent parameters were used in a new approach of stratified feature extraction for classifying karst, glacial, fluvial and denudational landforms. In this way, we have used stratified object-based image analysis to semi-automatically extract contrasting geomorphological features from high-resolution digital terrain data. A further step would be to also automate the optimization of classification rules. We would then be able to create a library of feature characteristics that could be transferred and applied to other mountain regions and further automate geomorphological mapping strategies.

1. Introduction

Technological advances in the last decade in remote sensing data acquisition and computational power have led to new types of data which are valuable for geomorphological research. For example Light Detection and Ranging (LiDAR) technology captures landscape topography in very high detail. Typically, LiDAR data is stored as point clouds or Digital Surface or Terrain Models (DSMs/DTMs) in geodatabases. A DTM is a grid cell-based representation of the land surface where vegetation and objects have been filtered out, thus representing bare-ground topography. Derivatives of LiDAR DTMs, also called Land-Surface Parameters (LSPs) (Hengl & Reuter, 2008) such as slope angle or shaded relief maps, have proven useful tools for mapping geomorphological features (e.g. McCormack et al., 2008; Arrowsmith & Zielke, 2009; Tarolli & Fontana, 2009).

DTMs and LSPs have been widely used for automated mapping and digital terrain analysis for a variety of applications, such as fluvial geomorphological research (Cavalli et al., 2008; Charlton et al., 2003; Milan et al., 2007; Thoma et al., 2005), landscape evolution modeling (Anders et al., 2009), landslide analysis (Van Den Eeckhaut et al., 2007; Glenn et al., 2006), lithological (Grebby et al., 2010) or geomorphological mapping (Seijmonsbergen et al., 2011; Van Asselen & Seijmonsbergen, 2006) and erosion monitoring (Roering et al., 2009).

Analysis of DTMs allows quantification of topography in a transparent, objective and systematic way (Hengl et al., 2008). Processing steps and work flows may be automated for the analysis of large datasets and with limited expert input. In this way, geomorphometrical analysis of DTMs can be used for automated classification of geomorphological features or processes, such as fluvially incised streams (e.g. James et al., 2007), landslides (e.g. Mantovani et al., 2010; Tarolli et al., 2008) and karst (e.g. Siart et al., 2009). Most of these techniques are based on training grid cells to determine key feature characteristics, which are used to classify larger areas (e.g. Prima et al., 2006). Traditional methods use grid cell or pixel-based classifications, which typically make them useful for analyzing low-resolution datasets covering large areas or homogeneous landscapes.

In the last decade, Object-Based Image Analysis (OBIA) has been generally accepted (Blaschke, 2010) as an effective tool for analyzing satellite images (Desclée et al., 2006; Walter, 2004) and high-resolution elevation data (Antonarakis et al., 2008; Drăguţ & Blaschke, 2006; Van Asselen & Seijmonsbergen, 2006). OBIA often uses a multi-

* Corresponding author.
E-mail address: N.S.Anders@uva.nl (N.S. Anders).

0034-4257/$ – see front matter © 2011 Elsevier Inc. All rights reserved.
doi:10.1016/j.rse.2011.05.007

resolution segmentation algorithm (Baatz & Schäpe, 2000) that clusters individual grid cells into image objects. Once the image objects are generated, they are classified using classification rules. In this way, object-based methods use groups of grid cells for classifications, which reflect how the human brain functions when identifying landscape features as objects (Blaschke & Strobl, 2001).

The size of image objects is controlled by a threshold – the scale parameter – which defines the maximum heterogeneity of grid cell values that is allowed within image objects. The more cells an image object contains, the more information is enclosed which can be used for classifying the specific image object. Obviously, when image objects become too large, they may enclose multiple target features which hinder accurate classification, which in turn leads to loss of detail. Image objects should, ideally, be of roughly the same size as, or slightly smaller than, the feature to be classified. Choosing an appropriate scale parameter value is therefore a crucial step.

Yet, segmentation parameter values and classification rules call for a manual trial-and-error optimization (e.g. Kim et al., 2008; Van Asselen & Seijmonsbergen, 2006; Blaschke et al., 2004). In this way, OBIA allows full control by the expert, but the degree of objectivity and automation is limited compared to pixel-based approaches.

In general, a low scale parameter value is necessary for extracting small features; a high scale parameter value is needed for extracting large features. We hypothesize that different geomorphological feature types require different sets of segmentation parameters. We define a 'geomorphological feature type' as all geomorphological features (i.e. landform or deposit) in an area that can be categorized within a specific unit of a legend, such as 'river terrace', or 'fluvial incision'. In complex landscapes however, small features are often intertwined with large features (e.g. small gypsum dolines within larger glacially eroded bedrock or mass movement features). We therefore argue that traditional OBIA (i.e. segmentation and classification of all feature types at once) may not give satisfying results when used for mapping entire areas of particular (complex) landscapes.

However, if stratified OBIA is applied, geomorphological feature types can be extracted separately. If segmentation parameters are optimized for each geomorphological feature type specifically, image objects can be generated that accurately follow specific feature boundaries. After a first feature type has been successfully extracted, subsequent image objects can be generated with different segmentation settings from which a second geomorphological feature type can be extracted. In this way, stratified OBIA may be used for analyzing high-resolution terrain data for the purpose of mapping an entire and complex landscape. Moreover, if the accuracy of image objects can be assessed automatically, we can automate the optimization of segmentation parameters. This will reduce manual trial-and-error procedures and increase the objectivity and classification accuracy.

In this paper we describe stratified OBIA of airborne LiDAR data as a new method for semi-automated mapping of geomorphological features. We present 1) a combined composite layer of multiple LSPs that was used as a mapping tool for creating reference datasets; 2) a novel method to assess the accuracy of image objects by means of a Segmentation Accuracy Assessment (SAA), which allowed optimization of image segmentation parameters; 3) a stratified feature extraction approach for classifying geomorphological features in a complex alpine catchment, and 4) a validation of the methods by comparing classification results with reference data.

2. Study area

The stratified OBIA approach was tested in an alpine catchment (approximately 10 km^2) in Vorarlberg, western Austria (Fig. 1). The area is drained by the river Gamp, and the elevation ranges from approximately 2170 m at the water divides to approximately 1630 m downstream. The current vegetation cover includes grasslands mixed with Norway Spruce (*Picea abies*) in the lower regions, and European Larch (*Larix decidua*) and Mountain Pine (*Pinus mugo*) in the higher areas.

The area is underlain by mainly limestone and dolomite formations belonging to the tectonic Lechtal and Arosa nappes. The area is characterized by the presence of remnants of mostly sedimentary rock (incl. gypsum) that is commonly associated with the base of the Lechtal nappe thrusts (Oberhauser, 1998; Ring et al., 1990). After full glaciation during the Würm, the glacially eroded bedrock slopes have been remodeled by Late-Glacial and post-glacial landform evolution and process activity. Current geomorphological processes include mechanical weathering, debris flows, rock fall, fluvial erosion and gypsum karst (Seijmonsbergen, 1992). The complex geological setting and geomorphological history have resulted in a wide variety of landforms and deposits, which made this a challenging test area for the semi-automatic classification of alpine geomorphology.

The geomorphological feature types that have been taken into account are: 1) glacially eroded bedrock, 2) ablation till, 3) fluvial incision, 4) river terrace or recent streambed, 5) deep-seated mass movement, 6) shallow mass movement, 7) fall deposits, 8) flow and/or slide deposits and 9) gypsum karst. These features add up to more than 99% of the total area.

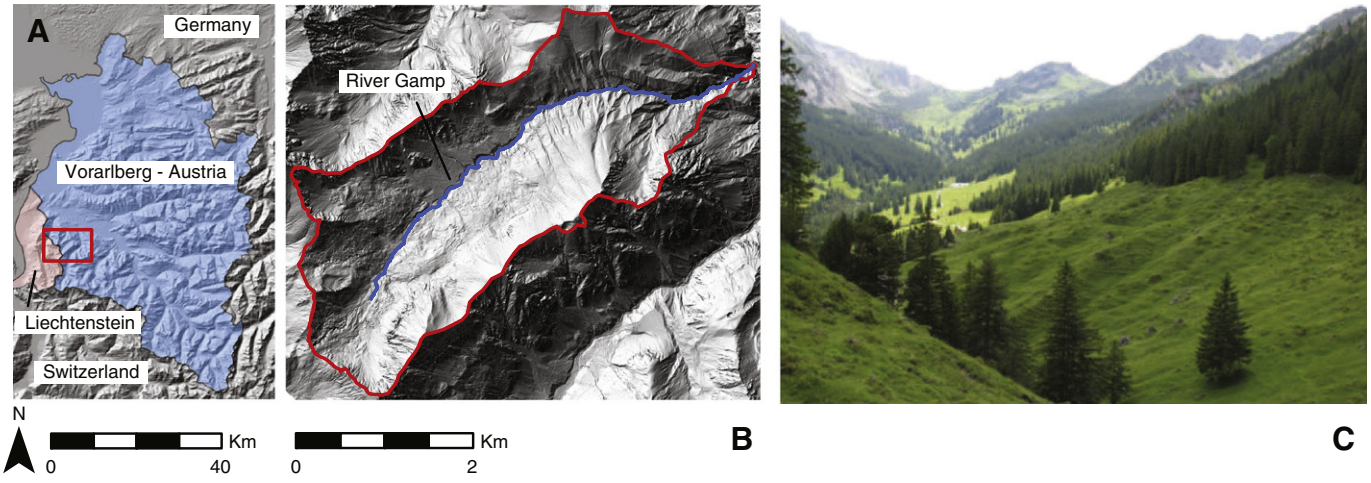

Fig. 1. A) The study area is located in the province of Vorarlberg, W-Austria (highlighted in blue) near the border of the Principality of Liechtenstein (highlighted in red) and Switzerland; The red square indicates the outline of the study area; B) The Gamp catchment is outlined in red, on top of a 1 m LiDAR DTM hillshade; C) The photo represents the complex geomorphological setting of the area: glacially eroded bedrock in the background, an incised river stream at the left and torrential debris flow deposits at the right.

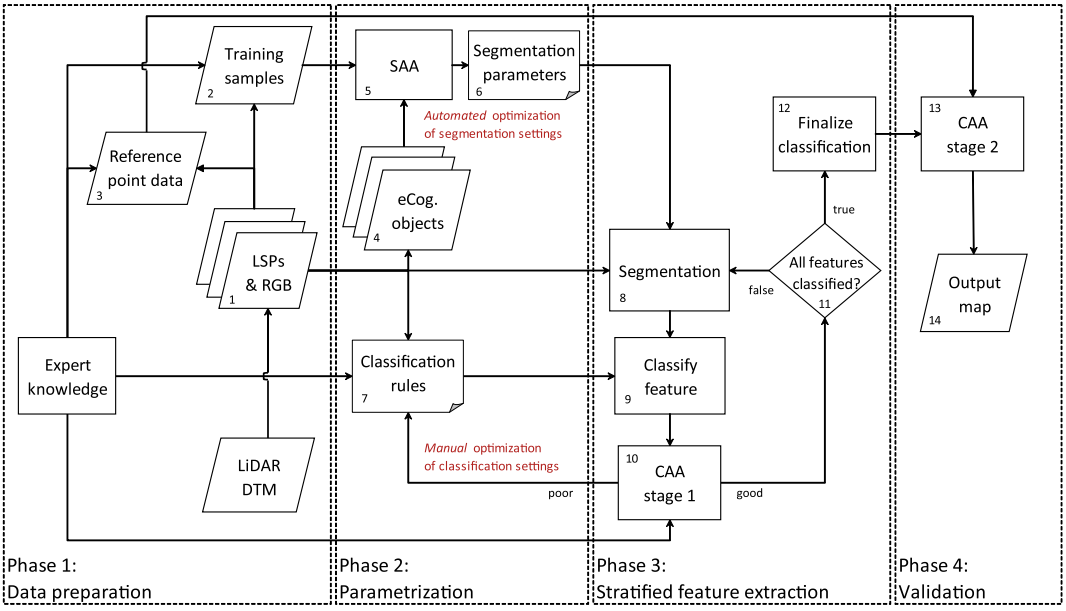

Fig. 2. Overview of the methods. The work flow is divided into four phases that correspond to the subchapters in the text, i.e. data preparation, parametrization, stratified feature extraction and validation. The numbers relate to the processing steps that are explained in the text.

3. LiDAR data acquisition and processing

Airborne LiDAR data of the study area was acquired between September and November 2004 with an Optech Airborne Laser Terrain Mapper (ALTM) 2050 scanner. From the raw point data, ground points were identified from non-ground points using a robust filtering approach, known as SCOP (Kraus & Otepka, 2005; Kraus & Pfeifer, 1998). Next, a 1 m DTM was created using linear least squares interpolation (Kraus & Mikhail, 1972). The data acquisition, filtering and DTM processing steps were carried out by the company TopScan.[1]

Based on visual inspection, the filtering of ground points was accurate throughout the entire catchment, except for areas that are very densely vegetated with Mountain Pine trees. These areas were situated in the highest regions near the water divides, of which the LiDAR DTM-derived LSPs returned irregular patterns that could not be linked with a natural morphology of the landscape. However, these filtering errors only existed very locally and did not hinder segmentation or classification results.

4. Methods

Fig. 2 summarizes the methods we used for the semi-automated classification of geomorphological features in the study area. The work flow is divided into four phases, with 14 processing steps in total. Phase 1 is necessary to create and prepare the data. Phase 2 deals with optimizing segmentation parameters and classification rule sets. Phase 3 executes a stratified segmentation and classification procedure based on the optimized parameters of phase 2. Phase 4 includes post-classification and validation steps, in order to produce the output map and to evaluate the classification results. Each processing step is explained.

4.1. Data preparation

Phase 1 consists of 1) calculating LSPs, 2) delineating training samples for the segmentation accuracy assessment and 3) creating a reference dataset for the classification accuracy assessment. This phase was carried out in ESRI ArcGIS software, and with python scripting for calculating terrain derivatives that are not included in the standard ArcGIS toolbox. Each step is explained.

In step 1, LSPs are calculated based on the LiDAR DTM. Many LSPs exist (Hengl & Reuter, 2008), of which some contain valuable information for geomorphological studies. The LSPs selected for this study are:

1. Slope angle, which is the key parameter that influences many gravity-driven geomorphological processes. Slope angle is calculated based on maximum rate of change in value from a cell to its direct neighbors in a 3×3 m window ((Burrough & McDonnell, 1998), p. 190).
2. Topographic openness, which represents the degree of enclosure of a location in the landscape (Yokoyama et al., 2002), and is calculated as the mean angle between a center cell and its surrounding cells in 8 directions. We calculated topographic openness within two search radii, namely 25 m (TO25) and 250 m (TO250). The TO25 parameter shows detailed topographic variation, while the TO250 parameter visualizes boundaries of geomorphological features.
3. Elevation percentile (EPC), which is the percentage of cells that are lower situated than a center cell in a given moving window (Gallant & Wilson, 2000). EPC contains information about the relative position of a location in the landscape. For example, a river terrace would be located relatively low in the landscape (EPC value of ~0.2–0.5) while a mountain ridge would be located relatively high (EPC value of ~0.7–0.9). Elevation percentile was calculated within a search radius of 250 m to match the window size of topographic openness to represent relative elevation at a larger scale than the individual features of interest.
4. A hydrologically conditioned DTM. Here individual sinks are filled in (Tarboton et al., 1991), originally to smoothen errors in digital elevation data for extracting channel networks, but real depressions are also filled in. If the altered DTM is subtracted from the original DTM, the filled area is highlighted which makes this LSP especially useful for locating gypsum karst.
5. Upstream area, which is used for identifying processes or landforms related to the flow of water (fluvial erosion and riverbed or terrace). The upstream area was calculated based on the widely used D8 single flow algorithm (O'Callaghan & Mark, 1984). In addition, a polyline representing the river Gamp was derived from the upstream area values. This was crucial for classifying fluvial features by calculating the distance of image objects to the main river.

[1] http://www.TopScan.de.

In step 2, training samples that are used for the segmentation accuracy assessment (SAA) in step 5 are selected and digitized. To achieve this, the slope angle, TO25 and TO250 parameters were combined as respectively red, blue and green layers into an RGB composite layer. By creating such a composite LSP layer, we were able to identify geomorphological features and their boundaries easier compared to using a traditional single-layer LSP such as shaded relief. In total we delineated three samples of nine different geomorphological feature types, which add up to 27 training samples.

In the third step, a reference point-based dataset is created that is used for the classification accuracy assessment (CAA, see step 13). Based on the RGB composite, in combination with a limited number of field checks, we manually classified over 600 points that were randomly distributed within the area's extent. The reference points were used to validate the classification results. More details on the validation are discussed in Section 4.4.

4.2. Parametrization

Once all data have been prepared, phase 2 assesses segmentation results and optimizes segmentation parameters and classification rules (steps 4–7). This phase was carried out using eCognition software for creating image objects and with python scripting in combination with ESRI geoprocessing tools for automating the parameter optimization. The following section presents all the steps in more detail.

In step 4, grid cells are clustered into image objects using a multi-resolution image segmentation algorithm (Baatz & Schäpe, 2000) of the eCognition software. The algorithm used slope and/or topographic openness (TO250) values as segmentation criteria for calculating the heterogeneity of cell values within image objects. This means that image object boundaries followed spatial patterns that exist within the slope and/or TO250 data, reflecting geomorphological feature boundaries. Multiple sets of objects were generated based on all possible combinations of these LSPs (i.e. only slope, only TO250 and slope in combination with TO250) and scale parameters of 2, 5, 10, 15, 20, 25, 30, 35, 40, 45, 50, 75, 100, 150, 200, 300, 400, 500, 750 and 1000. In this way, 60 unique sets of image objects were generated, each with a different combination of the segmentation parameters (i.e. scale parameter and LSPs).

In step 5, the quality of the segmentation results is evaluated for each specific geomorphological feature type, by means of a Segmentation Accuracy Assessment (SAA). Here, the automatically generated image objects are compared to the training samples of step 2. We calculated 2D frequency distribution matrices of slope angle and TO250 values of the training samples (Fig. 3A–B) and of image objects that intersect the training sample at a random location (Fig. 3C–H). The difference between the two frequency distribution matrices was used to calculate a normalized error (e):

$$e = \frac{H_f}{m} - \frac{H_o}{n} \tag{1}$$

where H_f is the frequency distribution matrix of the training sample, H_o is the frequency distribution matrix of the image object and m and n are the number of cells captured within a training sample and image object, respectively. We used an L_p norm (Dodge, 1987) to calculate the sum of absolute error (SAE) (Dielman, 2005):

$$SAE = \sum_{i=1}^{k} |e_i| \tag{2}$$

where k is the number of bins (i.e. 30×30). Since we delineated three training samples per geomorphological feature type, the final segmentation error (SE) was calculated based on the mean SAE. Segmentation errors were calculated for each set of image objects and for each geomorphological feature type. Subsequently, in step 6, the combination of LSPs and the scale parameter is selected for each specific geomorphological feature type that produced the smallest segmentation errors.

In step 7, the rule sets are developed for classifying the image objects. OBIA makes use of fuzzy classification rules, where the membership of objects to classes is being evaluated. The rules may consist of criteria of internal object statistics of grid cell values and mutual spatial relations between image objects (Definiens, 2009). We developed rule sets for each geomorphological feature type based on a long tradition of geomorphological mapping in alpine areas by staff members of the University of Amsterdam (De Graaff et al., 1987; Seijmonsbergen, 1992). An example of a rule set for a river terrace

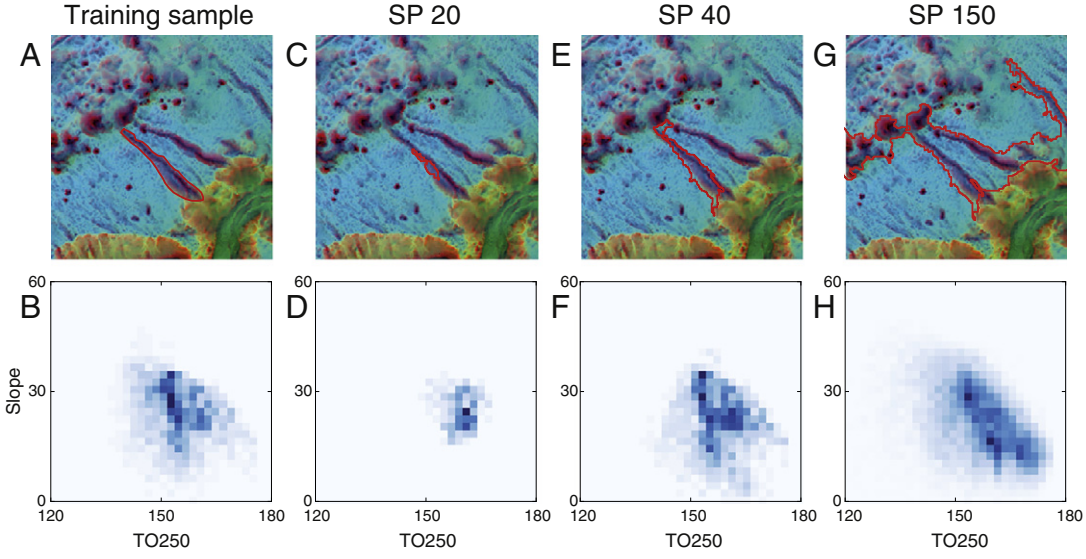

Fig. 3. An RGB composite of slope, TO25 and TO250 LSPs was used to manually delineate training samples. 2D frequency distribution matrices (with 30×30 bins) of training samples and image objects were calculated, based on the distribution of slope and TO250 values. A darker color in the frequency distribution matrices represents a higher occurrence. In this figure image objects generated with a scale parameter (SP) of 20, 40 and 150 are illustrated, of which SP40 best matches the training sample of a fluvial incision feature, in terms of both object boundaries and frequency distribution values.

would be a gentle slope (<10°), close to river stream (<50 m), and located low in the landscape (elevation percentile<0.5).

4.3. Stratified feature extraction

When the segmentation parameters and classification rule sets are determined, phase 3 performs the actual segmentation and classification (steps 8–12). Image objects are created *and* classified in a stratified way, which means that each geomorphological feature type is extracted separately, and in a predefined sequence. After optimal segmentation parameters are applied to accurately segment and subsequently classify the first feature type of interest, the remaining unclassified image objects are resegmented and classified in subsequent loops in order to extract the next geomorphological feature type of interest. A final step can be used to fill in remaining unclassified areas. This phase was carried out in eCognition software. Each step is briefly discussed below.

In step 8 the image objects are created based on optimal segmentation parameters of the geomorphological feature type of interest. In step 9 the classification rules are applied to determine the degree of membership (i.e. value ranging from 0 to 1) of image objects to the geomorphological feature type of interest. If the membership value exceeds a user-defined threshold (default is 0.1 for each feature type), the image object is classified as the target class.

In step 10, the classification accuracy of the specific geomorphological feature type is visually assessed, using expert knowledge based on RGB composite interpretation, and, if available, existing geomorphological maps. This step is necessary to quickly assess the quality of the classification in order to evaluate and fine-tune classification rules of the geomorphological feature type of interest. This step can also be used to manually edit erroneously classified image objects. In this way, the rule sets and the classification can be optimized for each feature type.

Step 11 checks whether all geomorphological feature types are processed. If false, the sequence starts again from step 8, where remaining unclassified image objects are resegmented based on the optimal segmentation parameters of the subsequent geomorphological feature type of interest, followed by object classification (step 9) and a feature-specific classification accuracy assessment (step 10).

Once all features are extracted, step 12 is used to finalize the classification. This step is optional, when there are still unclassified image objects present (i.e. left-over space). These areas are first segmented with average segmentation parameters, i.e. scale parameter of 50 and segmentation criteria 'slope and TO250'. Then the unclassified objects inherit the classification of neighboring features which they border most frequently. For example, if an unclassified image object shares 40% of its border with 'eroded bedrock', 25% with 'shallow mass movement' and 35% with 'fall deposits', then the unclassified object receives the classification 'eroded bedrock'.

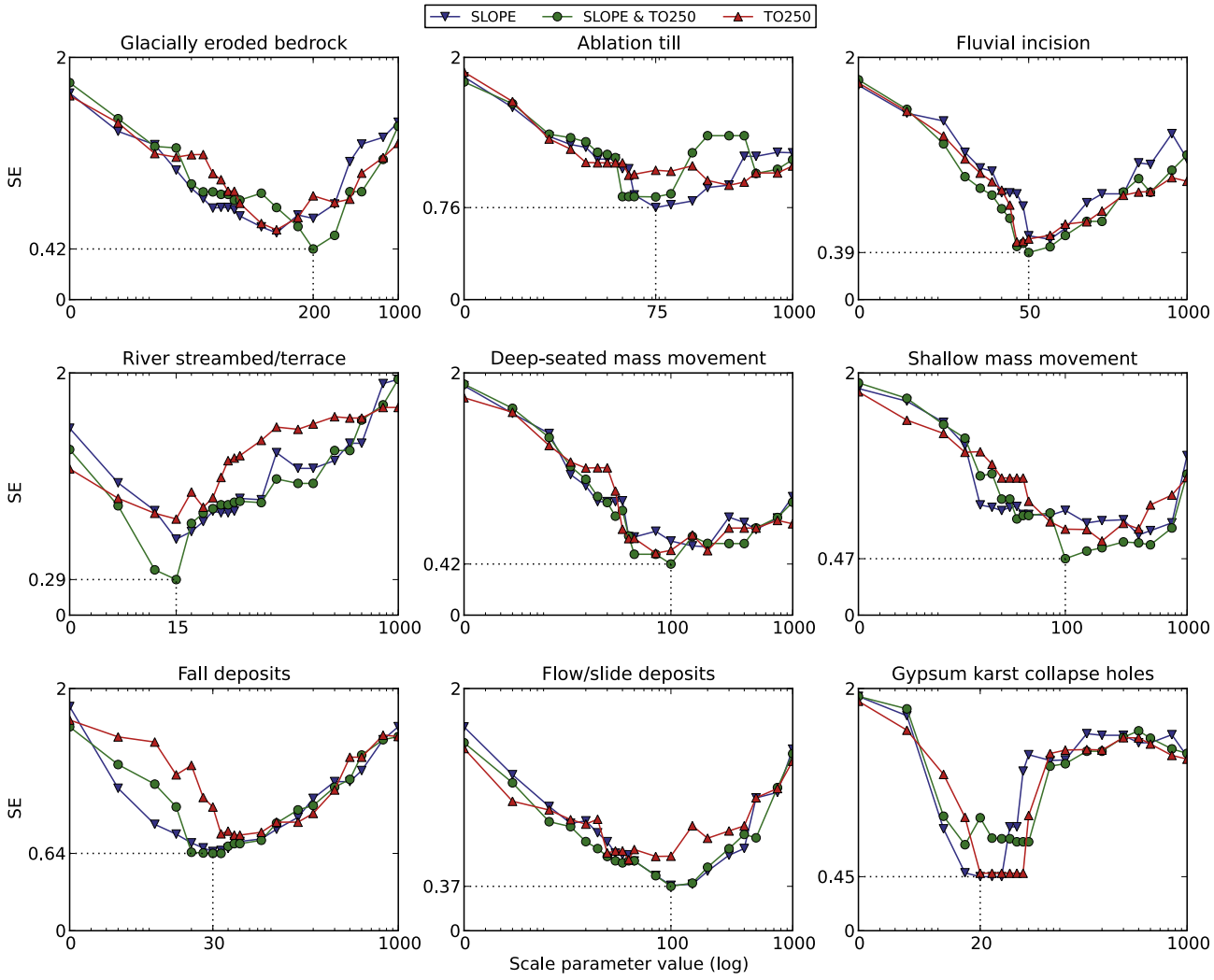

Fig. 4. The segmentation errors (*SE*) are plotted against the scale parameter. The blue, green and red lines indicate segmentation error calculated when respectively 'slope', 'slope and TO250' and 'TO250' were used as segmentation criteria. The error is calculated for each geomorphological feature separately. The smallest error values are highlighted at the axes of the subplots.

4.4. Validation

Phase 4 consists of the evaluation of the final classification results and the production of the output map. In step 13, the classification results are evaluated based on the reference point-based dataset of step 3. The classification results and the corresponding accuracy assessment comprised the final output map (step 14). The validation phase was carried out and automated with python in combination with ESRI geoprocessing tools.

5. Results

The results are presented in two subsections. The first section illustrates the segmentation parametrization results; the second section shows the implementation of stratified OBIA in eCognition and the classification results.

5.1. Segmentation parametrization

The goal of the parametrization phase was to assess segmentation results with respect to specific feature types, and to determine optimal segmentation parameters per geomorphological feature type. Fig. 4 shows the segmentation error per scale parameter and segmentation criteria for each geomorphological feature type. The parameter set with the smallest segmentation error value corresponds to the most accurate segmentation of the particular feature.

Optimal scale parameter values were found within the analyzed range (i.e. 1–1000). The results show that segmentation error gradually decreases with increasing scale parameter values, and increases again with larger values than the optimum, i.e. the optimal scale parameter. This optimal scale parameter value varies between 15 and 200, depending on geomorphological feature type.

The segmentation error values also vary between different segmentation criteria. This indicates that some LSPs are more suitable for segmentation than other LSPs. Most geomorphological feature types show the smallest segmentation error with the LSP combination 'slope and TO250', except for 'ablation till' and 'gypsum karst', where the smallest error values were calculated when objects are created based on respectively 'slope angle' and 'TO250' only.

The smallest segmentation error values also differ between geomorphological feature types. For example 'fluvial incision' receives the smallest error of 0.39, while 'ablation till' receives the smallest error of 0.76. This means that 'fluvial incision' is more accurately segmented than 'ablation till'.

5.2. Classification results

Table 1 presents an overview of the processing steps, parameters and values used in eCognition. The best classification results were

Table 1
Simplified process scheme illustrating how stratified feature extraction is implemented in eCognition and summarizing segmentation and classification settings per geomorphological feature type.

Geomorphological feature type	Processing step	Parameter	Criteria/value
River Gamp (hydrological feature)	Segmentation	LSPs	Slope and TO250
		Scale parameter	10
	Classify	Overlap river Gamp polyline	True
	Merge objects	Classified as	Unclassified
Recent riverbed or terrace	Segmentation	Classified as	Unclassified
		LSPs	Slope and TO250
		Scale parameter	15
	Classify	Distance to 'river Gamp', mean slope	Misc.
	Merge objects	Classified as	Unclassified
Fluvial incision	Segmentation	Classified as	Unclassified
		LSPs	Slope and TO250
		Scale parameter	50
	Classify	e.g. distance to 'river Gamp', mean slope, mean TO250, length/width ratio, mean EPC250, mean upstream area	Misc.
	Merge objects	Classified as	Unclassified
Gypsum karst	Segmentation	LSPs	TO250
		Scale parameter	20
	Classify	Area, filled in area, mean slope, mean TO25, mean TO250	Misc.
	Merge objects	Classified as	Unclassified
Glacially eroded bedrock	Segmentation	Classified as	Unclassified
		LSPs	Slope and TO250
		Scale parameter	200
	Classify	Mean EPC250, mean slope, mean TO250, standard deviation TO25	Misc.
	Merge objects	Classified as	Unclassified
Ablation till	Segmentation	Classified as	Unclassified
		LSPs	Slope
		Scale parameter	75
	Classify	Mean slope, mean TO250, standard deviation TO25	Misc.
	Merge objects	Classified as	Unclassified
Shallow mass movement	Segmentation	Classified as	Unclassified
		LSPs	Slope and TO250
		Scale parameter	100
	Classify	Mean slope, mean TO25, mean TO250	Misc.
Deep seated mass movement	Classify	Mean slope, mean TO25, mean TO250, standard deviation slope	Misc.
Flow or slide deposits	Classify	Mean EPC25, mean slope, mean TO250	Misc.
	Merge objects	Classified as	Unclassified
Fall deposits	Segmentation	Classified as	Unclassified
		LSPs	Slope and TO250
		Scale parameter	30
	Classify	Mean EPC250, mean slope, mean TO25, mean TO250	Misc.
n.a.	Fill in gaps	Borders most frequently to	All classes
	Export results	Classified as	All classes

produced when features were extracted in the following order: 1) recent riverbed or terrace, 2) fluvial incision, 3) gypsum karst, 4) glacially eroded bedrock, 5) ablation till, 6) deep-seated mass movement, 7) shallow mass movement, 8) flow/slide deposits and 9) fall deposits. Some feature types were created by combining multiple classes (i.e. fluvial incision, gypsum karst and glacially eroded bedrock). For example, 'fluvial incision' was combined from the classes 'fluvial incision by river Gamp' and 'fluvial incision by smaller streams'.

The final output map is presented in Fig. 5. The geomorphological map was imported into a geodatabase and prepared for further GIS applications. The accuracy assessment is presented in a confusion matrix (Congalton & Green, 1999), see Table 2. The classification was evaluated with an overall accuracy of 71% and a KHAT coefficient of agreement (Congalton & Green, 1999) value of 0.65. The user's and producer's accuracy (Congalton, 1991) indicate that some features are better classified than others. For example, 'glacially eroded bedrock' (74% and 88%), 'fluvial incision' (80% and 62%) and 'gypsum karst' (72% and 82%) are classified more accurately compared to 'shallow mass movement' (61% and 66%) and 'flow and/or slide deposits' (69% and 54%). Also 'ablation till' receives a relatively low user's accuracy (47%).

While the segmentation of e.g. 'flow/slide deposits' was determined relatively good (segmentation error of 0.37), it still received a relatively poor classification score, and the classification was often confused with 'deep-seated mass movement' and 'shallow mass movement'. This is likely the effect of overlapping classification rules and comparable LSP values within the objects. Better fine-tuning of the classification rules and including different classification criteria are necessary to improve the classification of flow/slide deposits features.

6. Discussion

6.1. RGB composite

Combining multiple LSPs into individual false-color composites for geomorphological research is only rarely used for visualizing and analyzing landscape features or processes (e.g. Hengl & Rossiter, 2003; Evans et al., 2009). Because multiple dimensions of information are summarized as a single color value (i.e. a combination of red, green and blue), the user first needs to become accustomed to the combined color values in order to correctly interpret the composite, for example by comparing spatial patterns to existing geomorphological maps. Once

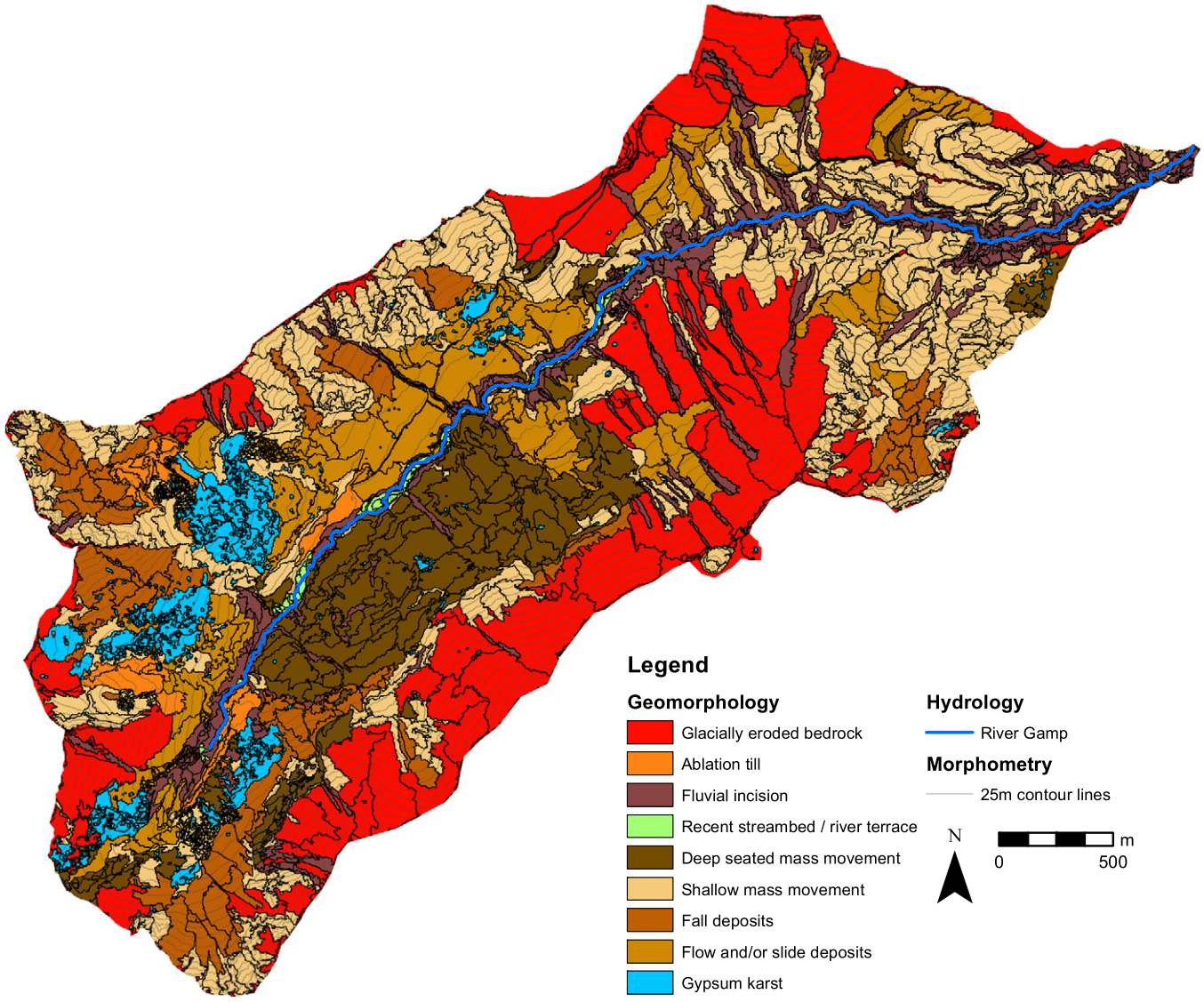

Fig. 5. The final map showing the geomorphological features. The legend has nine geomorphological classes, the location of the river Gamp and an overlay of LiDAR-derived 25 m contours.

Table 2
Comparison between the classification results and point-based reference data.

Reference data	Classification										User's accuracy [%]	Producer's accuracy [%]	Overall accuracy [%]	KHAT
	Gl. eroded bedrock	Ablation till	Fluvial incision	Recent river bed or terrace	Deep-seated mass mov.	Shallow mass mov.	Fal deposits	Flow/slide deposits	Gypsum karst	Total				
Gl. eroded bedrock	86	1	0	0	3	3	0	3	2	98	74	88	71	0.65
Ablation till	0	7	0	0	1	2	3	2	0	15	88	47		
Fluvial incision	5	0	47	2	1	19	0	2	0	76	80	62		
Recent riverbed or terrace	0	0	0	6	0	0	0	0	0	6	67	100		
Deep-seated mass mov.	0	0	2	0	69	8	1	4	3	87	74	79		
Shallow mass mov.	19	0	6	0	10	99	4	8	3	149	61	66		
Fall deposits	2	0	0	0	0	17	44	1	2	66	77	67		
Flow/slide deposits	5	0	4	1	8	11	5	44	3	81	69	54		
Gypsum karst	0	0	0	0	1	4	0	0	34	39	72	87		
Total	117	8	59	9	93	163	57	64	47	617				

the user adapts, spatial patterns in the RGB can more easily be linked with landforms and deposits, compared to patterns in single LSP layers such as shaded relief, slope or aspect. The RGB was found an important step in creating training samples to estimate segmentation accuracy, and in creating a reference dataset to estimate the accuracy of classification results.

The RGB consisted of slope angle, TO25 and TO250 because slope angle is an important parameter for geomorphological processes and topographic openness clearly visualizes geomorphological feature boundaries. When RGB composite analysis is used for other purposes than geomorphological mapping, different combinations of LSPs or other image layers are likely more effective.

6.2. Segmentation accuracy assessment

Image objects form the basis of a classification or map when applying OBIA. Classification results of a particular feature of interest will likely improve when image objects accurately follow feature boundaries, compared to classifications with poorly segmented objects. The assessment of segmentation results and the optimization of segmentation parameters may therefore improve classification results and the final map.

Automated estimation of scale parameter values was first introduced by (Drăguţ et al., 2010). They developed a tool that can be used for finding generally meaningful scale parameter values with a data-driven approach, for answering questions such as “What scales are present in the data?” Because we needed to answer questions such as “What scale parameter value creates the best objects for classifying specific geomorphological features?”, we needed to assess specific segmentation accuracy and could not use the tool mentioned. The quantitative comparison of frequency distribution matrices is a step forward towards the objective evaluation of segmentation accuracy. With our method, we can 1) assess the quality of objects with respect to specific features prior to the classification process and 2) optimize segmentation parameters. If image objects are created accurately, we can more efficiently optimize classification rules.

The shape of SE curves in Fig. 4 varies between relatively U-shaped and V-shaped curves. For example, a U-shaped curve as found with gypsum karst features illustrates a high segmentation accuracy within a relatively large range of scale parameter values. In other words, increasing the scale parameter value does not affect the size and shape of objects, until the objects are merged with neighboring objects, resulting in a rapid increase of SE. This means that the boundary of these features is relatively distinct. However, in V-shaped SE curves found with e.g. flow/slide deposits, the SE gradually changes with increasing scale parameter value. This represents a relatively fuzzy feature boundary. Therefore we argue that SE curves may be used for analyzing feature boundary fuzziness to further optimize classification strategies.

Only slope and TO250 values were used for calculating and comparing frequency distribution matrices. However, it is likely that the SAA will benefit from other or more LSPs. Therefore we suggest including a principal component analysis on numerous LSPs in future research, in order to find the optimal set of LSPs for analyzing multi-dimensional frequency distribution matrices. In addition, further tests are necessary to determine whether other LSPs are more suitable for creating image objects of relatively poorly delineated geomorphological features, or whether the topographic variation that is characteristic to these geomorphological features is poorly registered in the LiDAR dataset.

6.3. Stratified feature extraction

The SAA results indicate that different geomorphological feature types require different segmentation parameters. This means that, when all features are extracted at once using a single set of segmentation parameters, the overall classification accuracy will probably be low in areas with a complex geomorphological setting. We therefore argue that, when object-based image analysis is used, a stratified approach of feature extraction can be used for the accurate semi-automated mapping of geomorphology of entire complex landscapes. Alternatively, a multiscale approach may be used for mapping features with variable scale parameters. However, designing a meaningful ontology and/or hierarchy of multiscale features is much more complex and beyond the scope of this paper. Nevertheless, comparing stratified and multiscale approaches would be valuable for future research.

The sequence in which features are extracted greatly affects classification results. Based on a trial-and-error process, we generated best classification results when first smaller features with distinct boundaries are extracted, followed by larger features with fuzzy boundaries. This sequence is in line with classic field-based mapping strategies (e.g. De Graaff et al., 1987), where distinct features (e.g. fluvial incision) are drawn first, followed by features of which the boundaries are less clearly recognized in the field (e.g. mass movement terrain). However, while field-based techniques often tend to draw relatively young landforms and deposits prior to older geomorphological feature types, this is not necessarily true for stratified OBIA.

We estimated classification accuracies by calculating the percentage of correctly classified reference points. But, for example when shallow mass movement is confused with deep-seated mass movement, this is considered equally wrong as when shallow mass movement is confused with ablation till. The difference between the degree of error between the individual classes has not been incorporated. This should be taken

into account when interpreting the classification accuracy scores. In future research, we propose a weighted analysis of the confusion matrix, where errors between process domains (e.g. glacial and fluvial processes) are weighted heavier compared to errors within a single domain (e.g. shallow mass movement and deep-seated mass movement).

eCognition makes use of fuzzy rules and calculates membership values in each classification. In this study, individual feature types have been classified separately which means that we could not determine the degree of fuzziness of objects. The default membership threshold (0.1) used is therefore an arbitrary value, and increasing its value would likely give the same results when the classification rule values are set to a wider range. The membership threshold value should therefore be considered when interpreting the range of values of classification rules.

The final classification was assessed to have an average accuracy of 71% and a KHAT value of 0.65. The user's and producer's accuracies of the individual classes varied, which is likely caused by a combination of varying segmentation accuracy and the quality of classification rules. Although the current classification accuracies are not exceptionally high, it is a step forward to (semi-) automated geomorphological mapping at this scale of detail (compared to the scale of detail of e.g. the research of Prima et al., 2006). In addition, with stratified OBIA we were able to objectively map geomorphological features of an entire complex catchment, rather than mapping specific features (e.g. James et al., 2007; Glenn et al., 2006).

In order to improve the classification results we need to 1) improve the object segmentation by using different LSPs as segmentation criteria and 2) further optimize classification rules. As yet, the classification rule sets were optimized manually, but future work is planned to also automate the optimization of classification rule sets to increase the accuracy of individual feature classifications and the final geomorphological map. In this way, we can create a library of segmentation parameters and classification signatures per geomorphological feature type, that could be tested and applied to other regions.

The question remains whether automated techniques can completely replace traditional field-based methods. Many different field-based geomorphological mapping systems exist (e.g. De Graaff et al., 1987; Barsch & Liedtke, 1980; Gustavsson et al., 2008), of which most contain information on morphography, morphometry, morphogenesis, current processes, hydrography and the availability of unconsolidated materials. All sources contain vital information for understanding the geomorphological setting of an area. By using automated methods landscape analysis becomes more transparent, and if high-resolution data is used, feature boundaries are likely more accurately mapped compared to field-based maps. However, current automated methods of geomorphological mapping can only partly extract the information content of a geomorphological map, such as morphometry (Drăguţ & Blaschke, 2006) and hydrography (Tarolli & Fontana, 2009). In terms of equifinality, where landforms with a similar morphometry have different genesis, OBIA can be particularly valuable because of its ability to classify objects based on topological classification rules. In this way, spatial relations to other classified objects may help to improve our ability to classify morphogenetic characteristics of landscape objects.

7. Conclusions

Based on the results we conclude: 1) frequency distribution matrices provide crucial information for the assessment of image segmentation accuracy; 2) the segmentation accuracy assessment allowed automated optimization of segmentation parameters; 3) different geomorphological feature types have different optimal segmentation parameters for creating high-quality image objects of geomorphological features in an alpine landscape; and 4) a stratified approach of feature segmentation and classification is effective for the classification of geomorphological features in complex terrain; 5) the shape of SE curves may indicate the degree of fuzziness of particular features of interest, and may be used to improve classification strategies.

This research contributed to increasing the objectivity and efficiency of object-based analysis of high-resolution terrain data. Now we can more effectively apply digital landscape analysis for automated geomorphological mapping. This allows rapid analysis of the geomorphological setting of large areas to increase our understanding of the functioning of geo-ecological systems. In addition, segmentation parametrization and stratified feature extraction may also be valuable to other areas in the Earth sciences that use remotely sensed data, such as glacial research, lithological or land cover mapping, vegetation analysis, and forestry applications.

Acknowledgments

This research is financially supported by the Research Foundation for Alpine and Subalpine Environments (RFASE). In addition, it was carried out in the context of the Virtual Lab for e-Science (vl-e) project, which is supported by a BSIK grant from the Dutch Ministry of Education, Culture and Science (OC & W) and is part of the ICT innovation program of the Ministry of Economic Affairs (EZ). The 'Land Vorarlberg' has kindly allowed us to use the 1 m LiDAR DTM. We also thank 'inatura, Naturerlebnis Dornbirn' for their support. Guido van Reenen and the GIS-studio (www.gis-studio.nl) of the Institute for Biodiversity and Ecosystem Dynamics (IBED) are thanked for computational support.

References

Anders, N. S., Seijmonsbergen, A. C., & Bouten, W. (2009). Modelling channel incision and alpine hillslope development using laser altimetry data. *Geomorphology*, *113*, 35–46.

Antonarakis, A., Richards, K., & Brasington, J. (2008). Object-based land cover classification using airborne lidar. *Remote Sensing of Environment*, *112*(6), 2988–2998.

Arrowsmith, J. R., & Zielke, O. (2009). Tectonic geomorphology of the San Andreas Fault zone from high resolution topography: An example from the Cholame segment. *Geomorphology*, *113*(1–2), 70–81.

Baatz, M., & Schäpe, A. (2000). Multiresolution segmentation—An optimization approach for high quality multi-scale image segmentation. *Angewandte Geographische Informationsverarbeitung XII. Beiträge zum AGIT-Symposium Salzburg*, *200*, 12–23.

Barsch, D., & Liedtke, H. (1980). Principles, scientific value and practical applicability of the geomorphological map of the Federal Republic of Germany at the scale of 1:25 000 (GMK25) and 1:100 000 (GMK100). *Zeitschrift für Geomorphologie N.F. Supplement Band*, *36*, 296–313.

Blaschke, T. (2010). Object based image analysis for remote sensing. *ISPRS Journal of Photogrammetry and Remote Sensing*, *65*(1), 2–16.

Blaschke, T., Burnett, C., & Pekkarinen, A. (2004). Image segmentation methods for object-based analysis and classification. In S. M. De Jong, & F. D. Van der Meer (Eds.), *Remote sensing image analysis: Including the spatial domain* (pp. 211–236). Springer Netherlands: Remote Sensing and Digital Image Processing.

Blaschke, T., & Strobl, J. (2001). What's wrong with pixels? Some recent developments interfacing remote sensing and GIS. *GIS—Zeitschrift für Geoinformationssysteme*, *6*, 12–17.

Burrough, P. A., & McDonnell, R. A. (1998). Principles of geographical information systems. Oxford University Press.

Cavalli, M., Tarolli, P., Marchi, L., & Fontana, G. D. (2008). The effectiveness of airborne LiDAR data in the recognition of channel-bed morphology. *Catena*, *73*(3), 249–260.

Charlton, M., Large, A., & Fuller, I. (2003). Application of airborne LiDAR in river environments: The River Coquet, Northumberland, UK. *Earth surface processes and landforms*, *28*, 299–306.

Congalton, R. G. (1991). A review of assessing the accuracy of classifications of remotely sensed data. *Remote Sensing of Environment*, *37*(1), 35–46.

Congalton, R., & Green, K. (1999). Assessing the accuracy of remotely sensed data: Principles and practices. Boca Raton: Lewis Publsihers.

De Graaff, L. W. S., De Jong, M. G. G., Rupke, J., & Verhofstad, J. (1987). A geomorphological mapping system at scale 1:10,000 for mountainous areas. *Zeitschrift für Geomorphologie N.F.*, *13*(2), 229–242.

Definiens, A. G. (2009). Definiens eCognition developer 8 user guide.

Desclée, B., Bogaert, P., & Defourny, P. (2006). Forest change detection by statistical object-based method. *Remote Sensing of Environment*, *102*(1–2), 1–11.

Dielman, T. (2005). Least absolute value regression: Recent contributions. *Journal of statistical computation and simulation*, *75*(4), 263–286.

Dodge, Y. (1987). An introduction to L1-norm based statistical data analysis. *Computational Statistics & Data Analysis*, *5*(4), 239–253.

Drăguţ, L., & Blaschke, T. (2006). Automated classification of landform elements using object-based image analysis. *Geomorphology*, *81*(3–4), 330–344.

Drăguţ, L., Tiede, D., & Levick, S. (2010). ESP: A tool to estimate scale parameter for multiresolution image segmentation of remotely sensed data. *International Journal of Geographical Information Science*, *24*(4), 859–871.
Evans, I. S., Hengl, T., & Gorsevski, P. (2009). Applications in geomorphology. In T. Hengl, & H. Reuter (Eds.), *Geomorphometry — Concepts, software, applications. No. 33 in developments in soil science* (pp. 497–525). Amsterdam: Elsevier.
Gallant, J., & Wilson, J. (2000). Terrain analysis, principles and applications. *Primary topographic attributes* (pp. 51–85). John Wiley & Sons, Ch.
Glenn, N. F., Streutker, D. R., Chadwick, D. J., Thackray, G. D., & Dorsch, S. J. (2006). Analysis of lidar-derived topographic information for characterizing and differentiating landslide morphology and activity. *Geomorphology*, *73*, 131–148.
Grebby, S., Cunningham, D., Naden, J., & Tansey, K. (2010). Lithological mapping of the Troodos ophiolite, Cyprus, using airborne LiDAR topographic data. *Remote Sensing of Environment*, *114*, 713–724.
Gustavsson, M., Seijmonsbergen, A. C., & Kolstrup, E. (2008). Structure and contents of a new geomorphological GIS database linked to a geomorphological map — With an example from Liden, central Sweden. *Geomorphology*, *95*(3–4), 335–349.
Hengl, T., Najat, B., Blagojevic, D., & Reuter, H. (2008). Geostatistical modeling of topography using auxiliary maps. *Computers and Geosciences*, *34*, 1886–1899.
Hengl, T., & Reuter, H. (Eds.). (2008). *Geomorphometry: Concepts, software, applications. vol. 33*. Amsterdam: Elsevier.
Hengl, T., & Rossiter, D. G. (2003). Supervised landform classification to enhance and replace photo-interpretation in semi-detailed soil survey. *Soil Science Society of America*, *67*, 1810–1822.
James, L. A., Watson, D. G., & Hansen, W. F. (2007). Using LiDAR data to map gullies and headwater streams under forest canopy: South Carolina, USA. *Catena*, *71*(1), 132–144.
Kim, M., Madden, M., & Warner, T. (2008). Estimation of optimal image object size for the segmentation of forest stands with multispectral IKONOS imagery. In T. Blaschke, S. Lang, & G. Hay (Eds.), *Object-based image analysis—Spatial concepts for knowledge-driven remote sensing applications* (pp. 291–307). Springer.
Kraus, K., & Mikhail, E. (1972). Linear least squares interpolation. *Photogrammetric Engineering*, *38*(10), 1016–1029.
Kraus, K., & Otepka, J. (2005). DTM modelling and visualization—The SCOP approach. *Photogrammetric week (Heidelberg, 2005)* (pp. 241–252). Wichmann Verlag.
Kraus, K., & Pfeifer, N. (1998). Determination of terrain models in wooded areas with airborne laser scanner data. *ISPRS Journal of Photogrammetry and Remote Sensing*, *53*(4), 193–203.
Mantovani, F., Gracia, F., de Cosmo, P., & Suma, A. (2010). A new approach to landslide geomorphological mapping using the Open Source software in the Olvera area (Cadiz, Spain). *Landslides*, *7*, 69–74.
McCormack, D. C., Irving, D. H. B., Brocklehurst, S. H., & Rarity, F. (2008). Glacial geomorphological mapping of Coire Mhic Fhearchair, NW Scotland: The contribution of a high-resolution ground-based LiDAR survey. *Journal of Maps*, *2008*, 315–331.
Milan, D. J., Heritage, G. L., & Hetherington, D. (2007). Application of a 3D laser scanner in the assessment of erosion and deposition volumes and channel change in a proglacial river. *Earth surface processes and landforms*, *32*(11), 1657–1674.
O'Callaghan, J. F., & Mark, D. M. (1984). The extraction of drainage networks from digital elevation data. *Computer Vision, Graphics, and Image Processing*, *28*(3), 323–344.
Oberhauser, R. (1998). *Erläuterungen zur geologisch-tektonischen Übersichtskarte von Vorarlberg 1:200.000.* Wien: Geologische Bundesanstalt.
Prima, O. D. A., Echigo, A., Yokoyama, R., & Yoshida, T. (2006). Supervised landform classification of Northeast Honshu from DEM-derived thematic maps. *Geomorphology*, *78*(3–4), 373–386.
Ring, U., Ratschbacher, L., Frisch, W., DÜrr, S., & Borchert, S. (1990). The internal structure of the Arosa Zone (Swiss-Austrian Alps). *Geologische Rundschau*, *79*, 725–739.
Roering, J. J., Stimely, L. L., Mackey, B. H., & Schmidt, D. A. (2009). Using DInSAR, airborne LiDAR, and archival air photos to quantify landsliding and sediment transport. *Geophysical Research Letters*, 36.
Seijmonsbergen, A. C. (1992). *Geomorphological evolution of an alpine area and its application to geotechnical and natural hazard appraisal.* Ph.D. thesis. University of Amsterdam 109 pp.
Seijmonsbergen, A. C., Hengl, T., & Anders, N. S. (2011). Semi-automated identification and extraction of geomorphological features using digital elevation data. In M. Smith, P. Paron, & J. Griffiths (Eds.), Geomorphological Mapping: Methods and Applications Vol. 15 of Developments in Earth Surface Processes Elsevier, Amsterdam.
Siart, C., Bubenzer, O., & Eitel, B. (2009). Combining digital elevation data (SRTM/ASTER), high resolution satellite imagery (Quickbird) and GIS for geomorphological mapping: A multi-component case study on Mediterranean karst in Central Crete. *Geomorphology*, *112*(1–2), 106–121.
Tarboton, D., Bras, R., & Rodriguez-Iturbe, I. (1991). On the extraction of channel networks from digital elevation data. *Hydrological Processes*, *5*(1), 81–100.
Tarolli, P., Borga, M., & Fontana, G. D. (2008). Analysing the influence of upslope bedrock outcrops on shallow landsliding. *Geomorphology*, *93*(3–4), 186–200.
Tarolli, P., & Fontana, G. D. (2009). Hillslope-to-valley transition morphology: New opportunities from high resolution DTMs. *Geomorphology*, *113*(1–2), 47–56.
Thoma, D. P., Gupta, S. C., Bauer, M. E., & Kirchoff, C. (2005). Airborne laser scanning for riverbank erosion assessment. *Remote Sensing of Environment*, *95*(4), 493–501.
Van Asselen, S., & Seijmonsbergen, A. C. (2006). Expert-driven semi-automated geomorphological mapping for a mountainous area using a laser DTM. *Geomorphology*, *78*(3–4), 309–320.
Van Den Eeckhaut, M., Poesen, J., Verstraeten, G., Vanacker, V., Nyssen, J., Moeyersons, J., Van Beek, L. P. H., & Vandekerckhove, L. (2007). Use of LIDAR-derived images for mapping old landslides under forest. *Earth Surface Processes and Landforms*, *32*(5), 754–769.
Walter, V. (2004). Object-based classification of remote sensing data for change detection. *ISPRS Journal of Photogrammetry and Remote Sensing*, *58*(3–4), 225–238.
Yokoyama, R., Shirasawa, M., & Pike, R. J. (2002). Visualizing topography by openness: a new application of image processing to digital elevation models. *Photogrammetric engineering and remote sensing*, *68*(3), 257–265.